water

MDPI

*Article*

# Spatial Variations in Surface Snow Chemistry and Stable Isotope Composition Along Different Transects of the Antarctic Coastal Zone

**Yasheng Duan [1,2], Ming Yan [1,*], Zhong Chen [2,*], Robert Mulvaney [3], Weilong Huang [1], Chunlei An [1] and Leibao Liu [1]**

[1] Polar Research Institute of China, Shanghai 200136, China; m19945669824@163.com (Y.D.); hwl220@whut.edu.cn (W.H.); anchunlei@pric.org.cn (C.A.); liuleibao@pric.org.cn (L.L.)
[2] Department of Geosciences, Faculty of Land Resource Engineering, Kunming University of Science and Technology, Kunming 650093, China
[3] British Antarctic Survey, High Cross, Madingley Road, Cambridge CB3 0ET, UK; rmu@bas.ac
* Correspondence: mingyan@pric.org.cn (M.Y.); qwchenzhong@163.com (Z.C.)

**Abstract**

This study elucidated the spatial distribution characteristics of surface snow chemistry and stable isotope composition and their influencing factors in Antarctica's coastal region. We analyzed data from eight surface snow chemical ion transects and five surface snow stable isotope transects to examine the distributions of sea-salt ions ($Na^+$, $Cl^-$, $Mg^{2+}$, $K^+$), non-sea-salt ions ($NO_3^-$, methanesulfonic acid (MSA), non-sea-salt sulfate ($nssSO_4^{2-}$), non-sea-salt $Ca^{2+}$ ($nssCa^{2+}$)), and the stable isotope $\delta^{18}O$. Concentrations of chemical ions were found to exhibit distinct source signatures. Principal component analysis indicated that the ranking of ion sources in Antarctica's coastal areas is as follows: sea-salt aerosol transport, followed by marine biological activities and crustal dust and then atmospheric chemical reactions. Data from all transects exhibited a general pattern of diminishing $\delta^{18}O$ with increasing distance from the coast but with marked regional differences in the $\delta^{18}O$–distance slope (−6.84 to −1.98‰/100 km), $\delta^{18}O$–altitude slope (−0.97 to −0.20‰/100 m), and $\delta^{18}O$–temperature slope (0.61 to 1.14‰/°C). The moisture source regions and transport pathways, local orographic uplift, and local temperature field jointly affect the differentiation of $\delta^{18}O$ in coastal areas. The findings suggest that snow chemistry and isotopic composition in Antarctica's coastal zones are controlled by marine source transport, biogeochemical cycling, and polar topographic and climatic processes.

**Keywords:** Antarctica; snow chemistry; sea-salt ions; non-sea-salt ions; stable oxygen isotope; spatial variations



Academic Editor: Christos S. Akratos

Received: 4 June 2026
Revised: 30 July 2026
Accepted: 6 August 2026
Published: 9 August 2026



## 1. Introduction

Antarctic coastal areas lie at the forefront of interactions among ice, ocean [1], and the atmosphere. Influenced by factors such as the Antarctic Circumpolar Current, local marine cyclones, and ice-shelf melting, these areas have emerged as zones that are sensitively responsive to the effects of global climate change. Chemical ions and stable isotopes found in polar snow and ice serve as crucial indicators of contemporary climate processes and paleo-environmental changes [2]. In coastal areas, chemical ions in snow, such as sea-salt ions (primarily $Na^+$, $Cl^-$, $Mg^{2+}$, and $K^+$), originate from sea ice or seawater and are strongly influenced by sea ice extent and meteorological conditions [3,4]. Non-sea-salt ions,

including methanesulfonic acid (MSA), non-sea-salt sulfate ($nssSO_4^{2-}$), and non-sea-salt $Ca^{2+}$ ($nssCa^{2+}$), arise primarily from biological activities and crustal dust (wind-blown mineral particles from continental sources) [5], whereas $NO_3^-$ is generated by stratospheric sources [6]. Along coastal regions, the parameters describing $NO_3^-$ deposition—namely the dry deposition velocity and the scavenging ratio—remain relatively constant [7]. Stable isotopes, such as $\delta^{18}O$ and $\delta D$, indicate temporal and spatial variations in climate and are frequently employed to quantify historical changes in air temperature [8]. Deuterium excess (d-excess) serves as a second-order parameter that supports the identification of moisture source regions, effectively elucidating the formation mechanisms of polar precipitation and the evolution patterns of air masses [9].

A substantial body of baseline data on snow chemistry and stable isotopes have been collected across the Antarctic ice sheet. The International Trans-Antarctic Scientific Expedition (ITASE) provided a comprehensive synthesis of glacial chemical measurements for the entire ice sheet, most of which were obtained from surface snow [10]. During ITASE, numerous along-track studies measured snow chemistry and stable isotopes. These included traverses from Zhongshan Station to Dome A, from Dumont d'Urville Station (DDU) to Dome C, the coastal-to-interior traverse in Adélie Land, from Syowa Station to Dome F, and from Terra Nova Bay to Dome C, as well as the US ITASE in West Antarctica. Additional traverses comprised Italian routes, the Victoria Land traverse, and the Dronning Maud Land traverse [10,11]. Together, these efforts produced a large body of results on Antarctic surface snow chemistry. For example, chemical and isotopic analyses of samples collected along the route from Terra Nova Bay to Dome C demonstrated that surface snow chemistry exhibits substantial spatial variability [12]. This variability reflects changes in aerosol composition, wind scouring, and snowmelt processes at regional and local scales. The Russian Antarctic Expedition examined the spatial variability of sulfate ion and elemental concentrations and their fluxes in snow deposited along the transect from Progress Station to Vostok Station during 2006–2008 [13]. Concentrations of $Na^+$ and a fraction of $Mg^{2+}$ exhibited near-exponential decline with increasing inland distance and altitude, a pattern characteristic of sea-salt species. Sea-salt particles in snow can react with acids ($HNO_3$ or $H_2SO_4$) to form acid-modified sea-salt compounds [14]. A separate United States study in the Ross Sea region of West Antarctica found that both sea ice extent and the location of low-pressure systems affect the transport of sea-salt aerosols. Markedly, concentrations of sea salt and MSA in the snow pit at Siple Dome are substantially higher than at other inland sites at comparable distances from the coast [15]. This disparity indicates intensified low-tropospheric circulation in the Siple Dome region and stronger advection of marine air masses to that area. The stable isotope fractionation theory provides a fundamental framework for identifying water vapor sources in polar precipitation [16]. Through comprehensive analysis of Antarctic surface snow isotope data, Masson-Delmotte et al. (2008) clarified how the atmospheric circulation governs the spatial distribution of isotopes [17]. Comparative analyses across regions thus deepen our understanding of patterns and trends in the major chemical ions across Antarctica. Advances in observational techniques in recent years have shifted research toward ice sheet margins and coastal zones. However, our understanding of cross-disciplinary connections related to Antarctica's role in the Earth system (comprising the coupled atmospheric, oceanic, cryospheric, and biogeochemical processes that drive global climate) remains incomplete, especially around its coastal margins [18]. For example, Mulvaney and Wolff (1994) reported pronounced differences in ion sources between coastal and inland sites when examining the spatial variability of chemical constituents in the Antarctic ice sheet [19]. Additionally, Ding (2010) showed that the $\delta^{18}O$ distribution from Zhongshan Station to Dome A is controlled by altitude and temperature, with a gradient up to −1.1‰/100 m [20]. Recent work also

indicates that aerosol composition in Antarctic coastal regions is strongly affected by wind speed, with blowing snow processes providing a key mechanism for resuspending marine-derived ions [21]. Moreover, aerosols produced by sublimation of salts on the sea ice surface might represent a substantial material source for polar marine-origin chemistry [22].

However, marked deficiencies persist in existing research approaches. Most previous studies concentrated on a single cross section or local area [23]; thus, they lacked comparative analysis of the changes in chemical ions and stable isotopes across different coastal regions. Investigation of the spatial variations in chemical ions and stable isotopes remains insufficiently rigorous. Specifically, the synergistic effects of local processes, such as blowing snow and sea ice melting [24], as well as the impact of the large-scale circulation, require further clarification [25]. The complex terrain, diverse sources of water vapor, and robust interactions among the ice, ocean, and the atmosphere along the Antarctic coast might contribute to marked differences in the chemical characteristics of snow along various transects. However, the primary controlling factors behind these disparities have not been elucidated systematically. In response to the identified research gaps, this study examined surface snow chemical ions ($Na^+$, $K^+$, $Mg^{2+}$, $Ca^{2+}$, $Cl^-$, $SO_4{}^{2-}$, and $NO_3{}^-$) across eight transects, as well as $\delta^{18}O$ data from five transects along the Antarctic coast. By comparing the spatial variation patterns of chemical ions among different transects and integrating the water vapor source information revealed by stable isotopes, this research explored the comprehensive mechanisms via which factors such as marine aerosol input, atmospheric circulation transport, local topography, and biological activities influence the chemical characteristics of snow. The findings of this study provide essential data that support the enhancement of the observational network for climate and environmental changes in coastal regions of the Antarctic ice sheet. Furthermore, they offer a scientific foundation for deeper understanding of polar land–ocean interactions and coupling processes within the global climate system.

## 2. Study Areas, Data Collection, and Methods

### *2.1. Study Areas*

The study areas cover eight surface snow chemical ion transects and five surface snow stable isotope transects along the Antarctic coast. These transects are jointly influenced by marine aerosols, atmospheric circulation (including both wet and dry deposition processes), and local glacial processes (including katabatic wind redistribution, snow accumulation/erosion heterogeneity, blowing snow sublimation, and occasional surface melt–refreeze). The specific locations are shown in Figure 1. Information on the collection of surface snow data for the investigated transects is provided in Table 1.

**Table 1.** Information on the specific coastal transects on the Antarctic continent selected for consideration in this study. Here, transect identification is based on the initials of the actual transect names.

| Transect | Type | Sampling Date | Area | Reference |
|---|---|---|---|---|
| | | chemical ions [10] | | |
| Japan96-Japan114 (JJ) | surface snow | 1997 | EL | Bertler et al., 2005 [10] |
| Zhongshan–LGB69 (ZL) | surface snow | 2001–2002 | PEL | this study |
| T.-Talos_Dome (TT) | surface snow | 1987–2001 | AL | Bertler et al., 2005 [10] |
| D42-D80 (DD1) | surface snow | / | VL | Boutron and Lorius, 1997 [26] |
| pp-VLG1 (PV) | surface snow | 2000–2001 | VL | Bertler et al., 2005 [10] |
| Gl-CWA_D (GD) | surface snow | 1986–1995 | MBL | Bertler et al., 2005 [10] |

**Table 1.** *Cont.*

| Transect | Type | Sampling Date | Area | Reference |
|---|---|---|---|---|
| Dolleman Is.-DML′ (DD2) | surface snow | 1985–1998 | AP | Bertler et al., 2005 [10] |
| Finland1-Findland17 (FF) | surface snow | / stable isotope [17] | DML | Bertler et al., 2005 [10] |
| Zhongshan–LGB69 (ZL′) | surface snow | 2001–2002 | PEL | this study |
| Vostok1385-Vostok1033 (VV) | surface snow | 1964–1988 | KWL | Ekaykin et al., 2002 [27] Lipenkov et al., 1998 [28] |
| ITS7-ITS63 (II) | snow pits | 1998–1999 | VL | Frezzotti et al., 2005 [29]; Proposito et al., 2002 [12] |
| site1-site31 (SS) | surface snow | | AP | Qin et al., 1994 [30] |
| GvN 2 km Süd-DML75 (GD′) | snow pits | / | DML | Graf et al., 1994 [31]; Oerter et al., 1999 [32]; Graf et al., 1988 [33] |

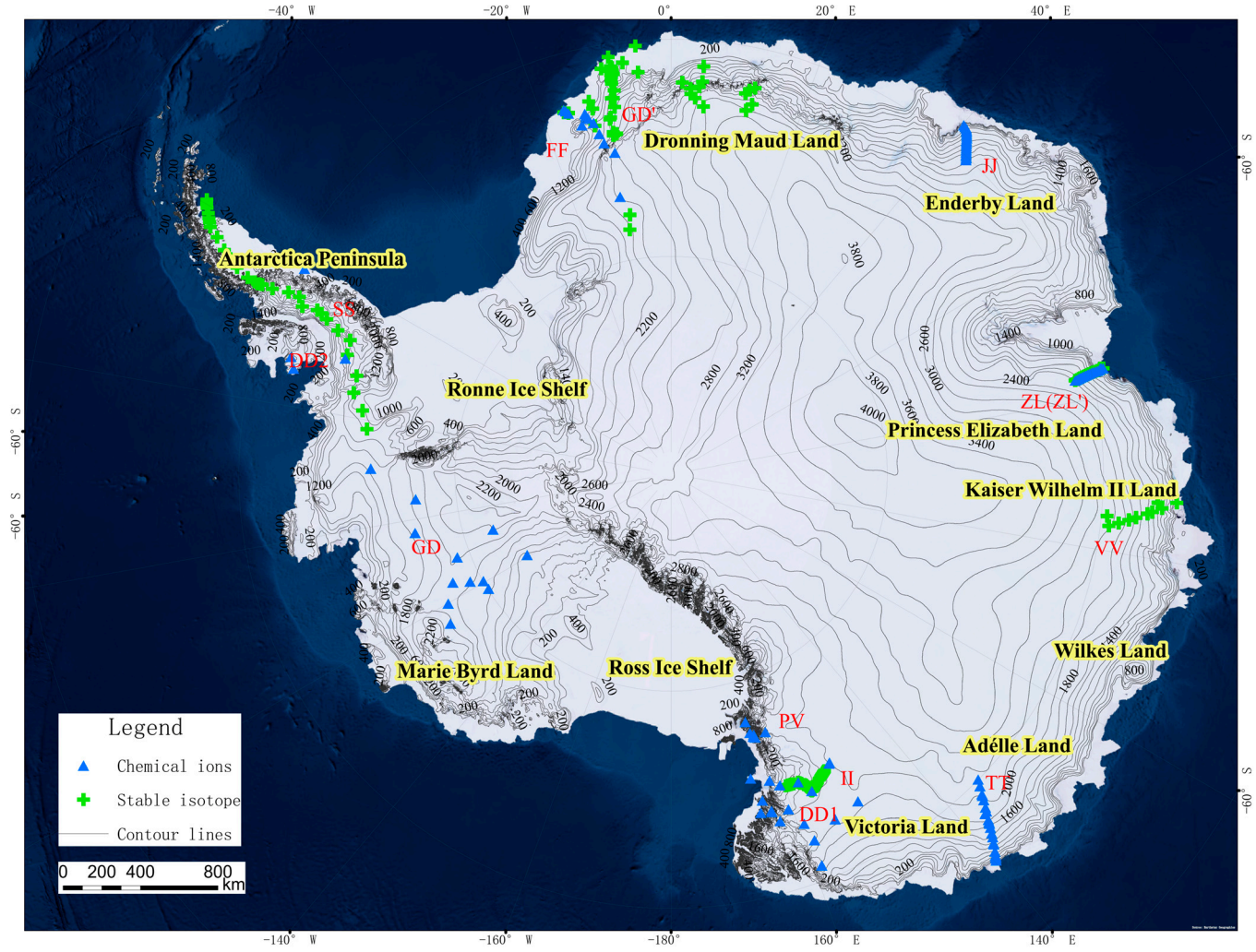


**Figure 1.** Locations of research transects in Antarctica.

### 2.2. Data Collection

The chemical ions ($Na^+$, $Cl^-$, $K^+$, $Ca^{2+}$, $Mg^{2+}$, $SO_4^{2-}$, $NO_3^-$, MSA, $nssSO_4^{2-}$, and $nssCa^{2+}$) were selected based on their established roles as tracers of distinct sources in Antarctic snow: sea-salt ions ($Na^+$, $Cl^-$, $K^+$, $Mg^{2+}$) indicate marine aerosol input; $nssSO_4^{2-}$ and MSA trace biogenic sulfur emissions; $nssCa^{2+}$ reflects terrestrial/crustal dust; and $NO_3^-$ serves as an indicator of atmospheric (stratospheric/tropospheric) sources. Stable

isotope $\delta^{18}O$ was included as a proxy for temperature, moisture source, and distillation history during transport. These variables collectively allowed us to quantify the relative contributions of different sources and to assess the spatial heterogeneity in both chemical ion distributions and isotopic signatures across the Antarctic coastal regions.

During the austral summer of the 18th CHINARE (Chinese National Antarctic Research Expedition, 2001–2002), we collected 17 surface snow samples along the transect from Zhongshan Station to LGB69 and analyzed them for major chemical ions and stable isotopes [34]. Detailed analytical procedures for chemical ions and stable isotopes (including sample preparation, ion chromatography (Dionex DX 500) and isotope (DLT-100) instrumentation, eluent conditions, calibration standards, and measurement uncertainties) are fully described in Huang et al. [34].

In addition to the chemical ion data from the Zhongshan–LGB69 (ZL) transect, we also used data from seven additional ITASE transects from the database (http://www2.umaine.edu/itase/content/syngroups/snowchem.html (accessed on 23 March 2026)) [10], which included the following ions: $Na^+$, $Cl^-$, $K^+$, $Ca^{2+}$, $Mg^{2+}$, $SO_4{}^{2-}$, $NO_3{}^-$, MSA, $nssSO_4{}^{2-}$, and $nssCa^{2+}$. The non-sea-salt fractions of $SO_4{}^{2-}$ and $Ca^{2+}$ were calculated using the following formula, assuming $Na^+$ originates solely from seawater:

$$nssSO_4{}^{2-} = SO_4{}^{2-} - Na^+ \times 0.2525 \quad (1)$$

$$nssCa^{2+} = Ca^{2+} - Na^+ \times 0.038 \quad (2)$$

where 0.2525 and 0.038 represent the mass concentration ratios of $(SO_4{}^{2-})/(Na^+)$ and $(Ca^{2+})/(Na^+)$ in seawater, respectively [34].

We also used stable isotope data from 17 samples collected along the route from Zhongshan Station to LGB69, and from four additional transects. The reference stable isotope data for the VV, II, SS and GD' transects were obtained from the Antarctic surface snow isotope composition database (https://doi.pangaea.de/10.1594/PANGAEA.681697, (accessed on 23 March 2026)) [17]. Detailed information on surface snow chemical ion and stable isotope data is presented in Table 1.

### *2.3. Methods*

The sampling datasets comprised data from surface snow on eight ion transects and five isotope transects from coastal areas of Antarctica. They provided a basis for analyzing the spatial distribution of sea-salt and non-sea-salt ions, as well as the regional differences in their sources. The driving mechanisms behind these spatial heterogeneities remain unclear. To address this problem, this study applied the following approaches: (1) use the enrichment factor (EF) to distinguish sea-salt from non-sea-salt ion sources; (2) employ principal component analysis (PCA) for dimensionality reduction to extract the dominant factors controlling variations in chemical composition; and (3) combine $\delta^{18}O$–distance, $\delta^{18}O$–altitude, and $\delta^{18}O$–temperature slope relationships to evaluate differences in stable isotope fractionation among coastal transects. The specific method of each of these three approaches is described as follows.

#### 2.3.1. Enrichment Factor

The enrichment factor (EF) quantifies the degree to which an element is enriched in a sample. This calculation relies on the elemental ratio of ions collected from the atmosphere or precipitation compared with the corresponding ratio in a reference material [35]. In coastal Antarctica, however, blowing snow can substantially redistribute and fraction-ate ions, which may affect the reference $Na^+$ concentration and consequently the calculated EF values. This potential limitation should be considered when evaluating the EF results,

particularly for wind-exposed sites. To identify the sources of ions in surface snow, we utilized the EF to compare the relative concentrations of elements ($Cl^-$, $K^+$, $Mg^{2+}$, $Ca^{2+}$, and $SO_4^{2-}$) in Antarctic snow with those found in seawater. In this study, $Na^+$ was used as an indicator of seawater spray under the assumption that seawater spray is the sole source of $Na^+$, with no selective fractionation or post-deposition effects. The EF for the ionic component X is calculated as follows:

$$EF(X) = ([X]/[Na^+])_{snow}/([X]/[Na^+])_{seawater} \quad (3)$$

where ([X]/[$Na^+$])snow represents the ratio of the concentration of any ionic component in the analyzed snow to that of $Na^+$, while ([X]/[$Na^+$]) seawater denotes the ratio of these ionic components in seawater. An EF value of >1 indicates that the ion is enriched relative to seawater, suggesting additional contributions from non-marine sources (e.g., long-distance transported mineral dust, biological emissions, or atmospheric chemical reactions), whereas an EF value of <1 suggests that some fractionation or depletion relative to seawater has occurred. According to the generalized major ion composition of seawater, the seawater ([A]/[$Na^+$]) reference values used in this study were 1.8 for $Cl^-/Na^+$, 0.037 for $K^+/Na^+$, 0.12 for $Mg^{2+}/Na^+$, 0.038 for $Ca^{2+}/Na^+$, and 0.25 for $SO_4^{2-}/Na^+$; there are no clear standards for the reference values of $NO_3^-/Na^+$ and MSA/$Na^+$ in seawater (because their concentrations in seawater are extremely low) [36].

There were only data on $Na^+$, $Cl^-$, and $NO_3^-$ in the DD1 transect, and these data cannot be used for determination of the EF value. Therefore, this method was not used for analysis of the DD1 transect.

#### 2.3.2. Principal Component Analysis

Principal component analysis (PCA) is a statistical method that reduces the dimensions of high-dimensional data through orthogonal transformation. Its core purpose is to reduce the number of variables while retaining the main features of the data. This method converts the original variables into uncorrelated principal components (PCs) by calculating the eigenvectors (i.e., principal component loads) and eigenvalues (representing the variance contribution rates of each PC) of the covariance matrix. The first PC (PC1) explains the maximum variance in the data, and the subsequent PCs decrease in sequence. PCA is used widely in the field of environmental geochemistry research to identify pollutant sources and mixing processes [37].

Here, PCA was applied to identify the primary factors driving changes in chemical ion concentrations. Prior to PCA, all ion concentration data were standardized using z-score normalization to ensure equal weighting of variables. PCA was applied to the eight chemical ion transects in the study area. For the PV and DD1 transects, the cumulative variance explained by the PCs did not exceed 80%; therefore, these two transects were deemed unsuitable for PCA-based interpretation. Consequently, the final analysis was restricted to the remaining six transects.

#### 2.3.3. $\delta^{18}O$–Distance, $\delta^{18}O$–Altitude, and $\delta^{18}O$–Temperature Slopes

The spatial distribution of stable isotopes ($\delta^{18}O$) in Antarctic surface snow provides critical proxies for reconstructing regional climate and hydrological processes. The spatial variations in $\delta^{18}O$ are strongly related to the spatial variation in temperature, which is strongly related to distance from the open ocean (continentality effect), latitude (link with insolation), altitude (vertical lapse rate effect), and atmospheric circulation (penetration of synoptic cyclonic systems). Temperature data for the isotope transects were obtained from the same source databases, which provide 10 m firn temperature measurements. These measurements are widely used as a proxy for mean annual air temperature in

Antarctic studies [17]. The spatial variation in $\delta^{18}O$ is closely associated with temperature variation; because temperature fluctuates a lot due to other factors, we excluded some outliers. We calculated the slopes of the $\delta^{18}O$–temperature relationship at five transects using linear regression to convert the isotope data into a temperature scale. This study also calculated the slopes of $\delta^{18}O$ versus distance and $\delta^{18}O$ versus altitude. The $\delta^{18}O$–distance slope captures the Rayleigh fractionation during the transport of moisture inland and thus characterizes the linkage between source and precipitation regions. The $\delta^{18}O$–altitude slope captures the condensation effects driven by orographic uplift, thereby reflecting vertical climatic differentiation [38].

## 3. Results

### *3.1. Spatial Distribution and Source Analysis of Chemical Ions*

#### 3.1.1. Spatial Distribution of Chemical Ions

The variation in major ion concentrations with altitude along the eight transects (Figure 2a–h) reveals pronounced regional differences in sea-salt ions ($Na^+$, $Cl^-$, $Mg^{2+}$, $K^+$) with altitude across the coastal zones of Antarctica. In the low-altitude (0–600 m) segment of the ZL transect in the PEL of East Antarctica (Figure 2b), sea-salt ion concentrations reach their maximum ($Na^+$: 970.78–1458.92 ppb; $Cl^-$: 952.48–1659.08 ppb; $K^+$: 10.51–20.45 ppb; $Mg^{2+}$: 46.22–76.56 ppb). The overall concentration of sea-salt ions of the DD1 transect within the VL region of East Antarctica (Figure 2d) is the lowest ($Na^+$: 4.6–437 ppb; $Cl^-$: 14–108.5 ppb). Moreover, the spatial patterns of sea-salt ions ($Na^+$, $Cl^-$, $Mg^{2+}$, $K^+$) across the transects of East Antarctica (JJ, ZL and TT transects) are essentially identical (Figure 2a–c), all showing exponential decline with increasing altitude, which is a typical characteristic of the variation in sea-salt ions [39]. In the coastal regions of West Antarctica, sea-salt ion concentrations decrease markedly with increasing altitude. Specifically, the sea-salt ion concentrations of the PV transect are substantially higher ($Na^+$: 2802 ppb, $Cl^-$: 1314 ppb, $K^+$: 100.1 ppb, $Mg^{2+}$: 331.4 ppb; Figure 2e) than those of the GD transect ($Na^+$: 406.1 ppb, $Cl^-$: 799.7 ppb, $K^+$: 31.3 ppb, $Mg^{2+}$: 66.1 ppb; Figure 2f). The concentrations of sea-salt ions along the coastal transects in East Antarctica are generally higher than those in West Antarctica. In contrast, the AP exhibits consistently high values without any clear trend (Figure 2g).

The spatial distribution of non-sea-salt ions ($NO_3^-$, MSA, $SO_4^{2-}$ and $Ca^{2+}$) along the eight coastal transects also varies significantly. $NO_3^-$ concentrations range from 8 to 200 ppb. The minimum value occurs on the ZL transect (8.55 ppb; Figure 2b), and the maximum value occurs on the FF transect (207.4 ppb; Figure 2h). $NO_3^-$ concentrations do not follow a systematic pattern with altitude. $SO_4^{2-}$ concentrations ranged from 10 to 450 ppb. Along the JJ transect (Figure 2a), concentrations are relatively low (15.1–37.4 ppb). Concurrently, the contribution of $nssSO_4^{2-}$ in the high-altitude zone of the JJ transect is higher than that along other transects, primarily reflecting stratospheric sulfate from volcanic eruptions or dimethyl sulfide (DMS) oxidation [40,41]. MSA concentrations vary from 2 to 150 ppb. Along the ZL transect, values are highest overall (2.77–145.82 ppb), likely driven by intense regional biological activity and strong phytoplankton blooms [34]. Broadly, MSA mirrors the pattern of $nssSO_4^{2-}$ (Figure 2b). Concentrations of $Ca^{2+}$ and $nssCa^{2+}$ are generally low but stable across the study area, indicating long-range continental dust input [34].

#### 3.1.2. Source Analysis of Chemical Ions

Analysis of EFs for five ions ($Cl^-$, $SO_4^{2-}$, $Ca^{2+}$, $K^+$, $Mg^{2+}$) in surface snow from the seven coastal Antarctic transects (excluding DD1; Figure 3a–g) reveals both regional commonalities and pronounced spatial variability. The EF($Cl^-$) and EF($Mg^{2+}$) values are

close to 1 across all transects, consistent with seawater sources, indicating derivation mainly from sea-salt aerosols. The EF($SO_4^{2-}$) and EF($Ca^{2+}$) values exceed 1 markedly along each transect, indicating non-seawater enrichment, i.e., mostly from sources other than marine aerosols. The EF($K^+$) values on the JJ, TT and FF transects are substantially greater than 1, implying additional sources beyond seawater (Figure 3a,c,g).

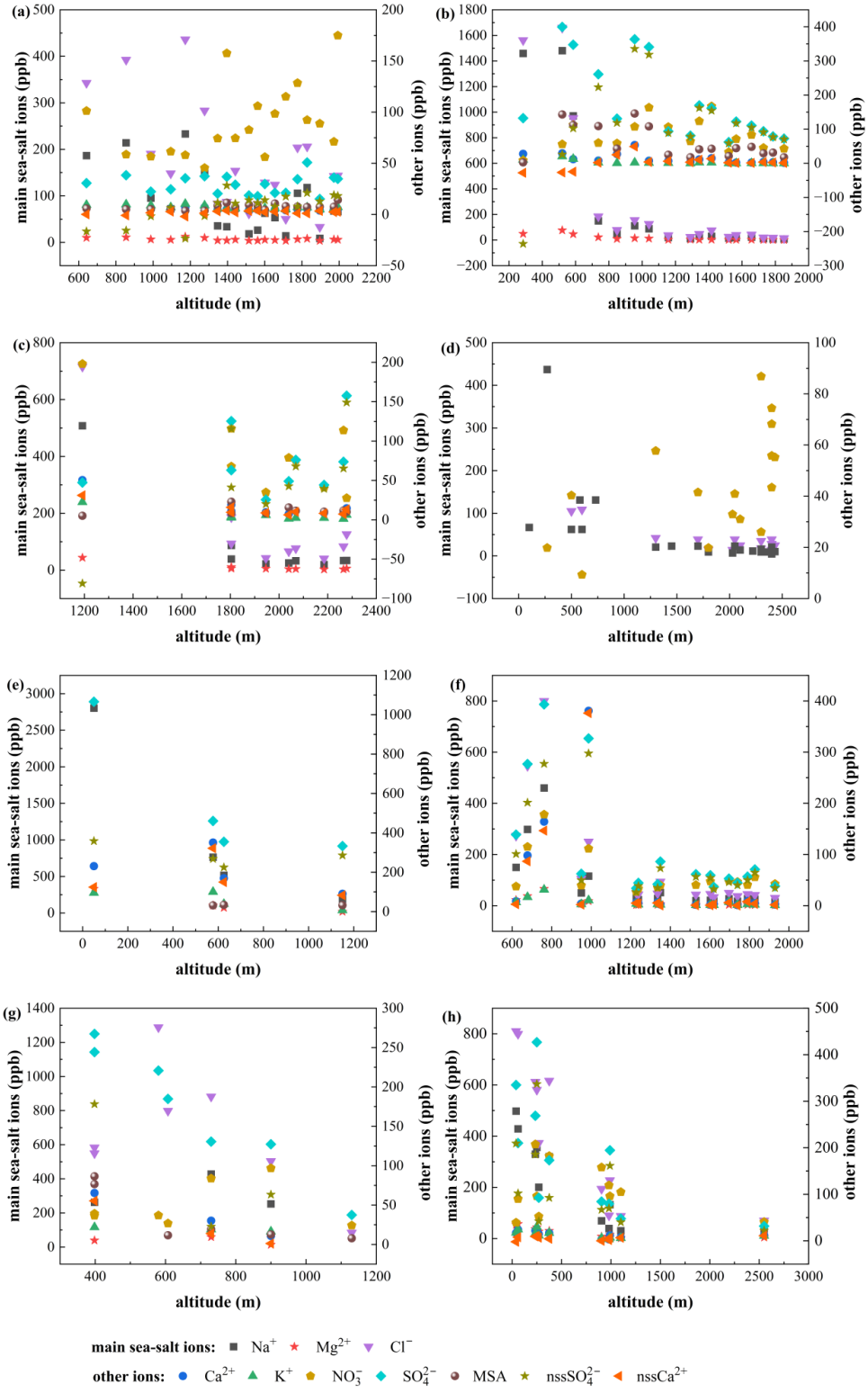


**Figure 2.** Variation in chemical ion concentrations with altitude for each transect: (**a**) JJ transect, (**b**) ZL transect, (**c**) TT transect, (**d**) DD1 transect, (**e**) PV transect, (**f**) GD transect, (**g**) DD2 transect, and (**h**) FF transect.

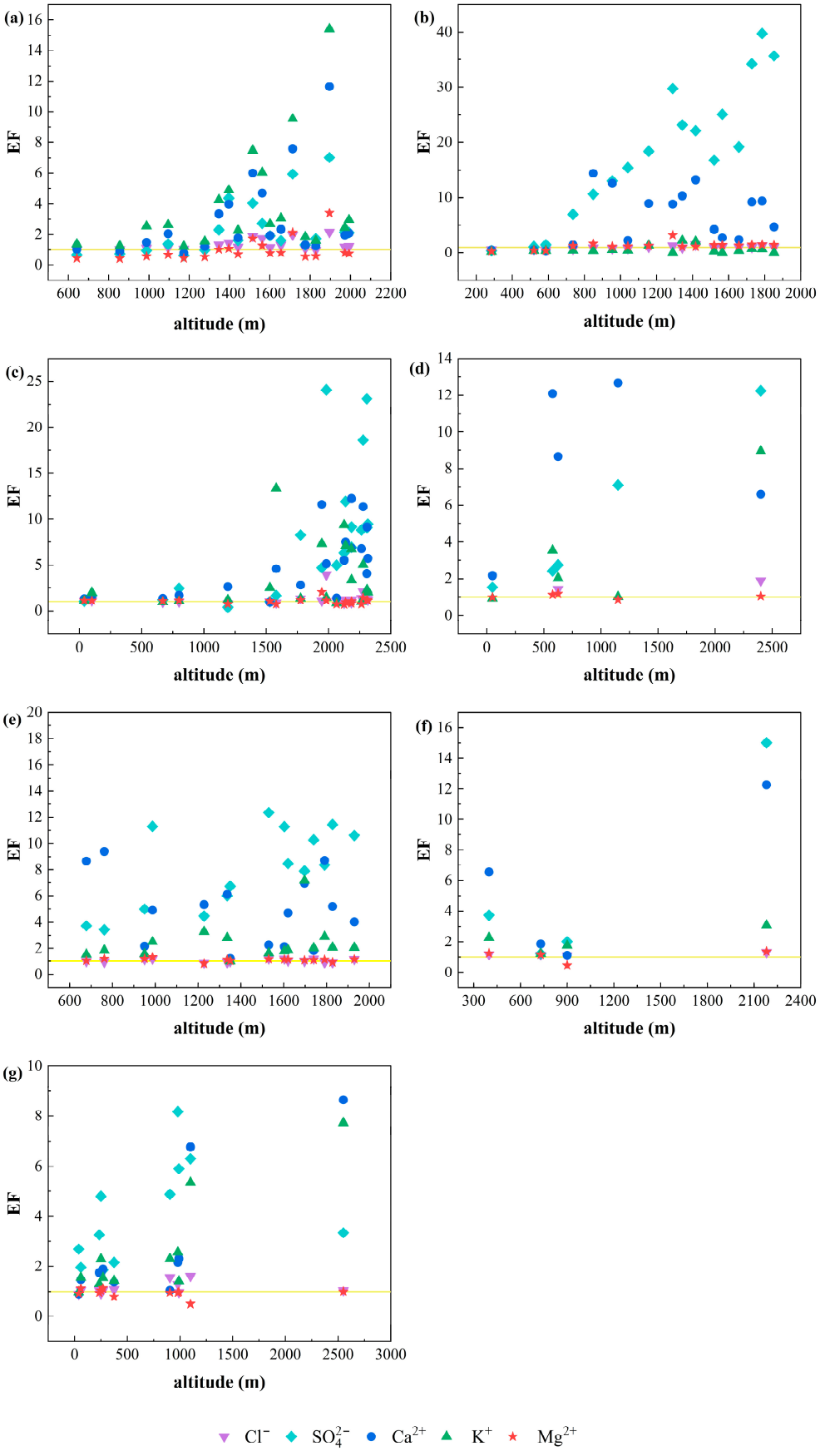


**Figure 3.** Enrichment factor (EF): (**a**) JJ transect, (**b**) ZL transect, (**c**) TT transect, (**d**) PV transect, (**e**) GD transect, (**f**) DD2 transect, and (**g**) FF transect.

We conducted PCA on the data obtained from six transects, excluding the DD1 and PV transects (Table 2). The results indicate substantial differences in the variances of PC1, PC2, and PC3 across the transects, but the PC values all exhibit a trend of reduction. Specifically, PC1 accounts for the largest variance contribution rate, ranging from 53.00% to 73.54%, followed by PC2, which contributes between 14.42% and 31.10%, and then PC3, which has the smallest contribution, ranging from 11.40% to 13.62%. For the JJ transect, PC1 exhibits a high positive loading of sea-salt ions, while PC2 is characterized by MSA (0.624) generated by marine biological activities and $NO_3^-$ (0.795) generated by atmospheric chemical reactions. For the ZL transect, although PC1 is also dominated by sea-salt components, PC2 includes MSA (0.821) and $nssSO_4^{2-}$ (0.873), which are indicators typical of marine biological activities. For the TT transect, PC1 and PC2 are influenced predominantly by $nssCa^{2+}$ (0.813) and $nssSO_4^{2-}$ (0.814), respectively, suggesting origins in crustal dust and marine biological activities. Conversely, for the GD transect, the substantial loadings of $nssSO_4^{2-}$ (0.949) and $SO_4^{2-}$ (0.884) in PC2 indicate atmospheric chemical reactions driven by marine biological activities and volcanic eruptions. The DD2 transect exhibits a distinct pattern compared with the other transects. In PC1, the indicators of crustal dust and biological activities, including $nssCa^{2+}$ (0.922), MSA (0.96), $SO_4^{2-}$ (0.973), and $Ca^{2+}$ (0.985), surpass those of sea-salt ions, while PC2 is dominated by sea-salt ions. These findings suggest that the sources of chemical ions along the Antarctic coast are governed primarily by three processes: sea-salt aerosol transport (dominating PC1), marine biological activities and crustal dust (dominating PC2), and atmospheric chemical reactions (partially represented in PC3). The anomalous pattern observed in the DD2 transect might be influenced by its unique local environment or specific sampling conditions. For the FF transect, PC1 exhibits a high positive loading of sea-salt ions, while PC2 is characterized by crustal dust $nssCa^{2+}$ (0.973), and PC3 is associated with $NO_3^-$ (0.965) generated by atmospheric chemical reactions.

**Table 2.** Principal component analysis of six transects.

| | | $Mg^{2+}$ | $Cl^-$ | $Na^+$ | $K^+$ | $nssCa^{2+}$ | $nssSO_4^{2-}$ | MSA | $SO_4^{2-}$ | $NO_3^-$ | $Ca^{2+}$ |
|---|---|---|---|---|---|---|---|---|---|---|---|
| JJ | | | | | | | | | | | |
| PC1 | 73.54% | **0.985** | **0.989** | **0.991** | **0.949** | **−0.962** | **−0.864** | −0.68 | 0.546 | −0.465 | **0.935** |
| PC2 | 15.88% | 0.131 | 0.115 | 0.119 | 0.101 | −0.069 | 0.279 | 0.624 | 0.63 | **0.795** | 0.182 |
| ZL | | | | | | | | | | | |
| PC1 | 53.90% | **0.994** | **0.982** | **0.98** | **0.976** | −0.66 | −0.425 | 0.479 | 0.629 | −0.222 | 0.481 |
| PC2 | 31.10% | 0.046 | −0.147 | −0.16 | 0.036 | 0.559 | **0.873** | **0.821** | **0.755** | 0.691 | 0.511 |
| TT | | | | | | | | | | | |
| PC1 | 53.00% | **0.912** | **0.93** | **0.94** | **0.83** | 0.384 | −0.099 | 0.47 | **0.898** | 0.011 | **0.92** |
| PC2 | 19.69% | −0.397 | −0.358 | −0.334 | 0.329 | **0.813** | 0.446 | 0.686 | −0.124 | 0.203 | 0.277 |
| PC3 | 13.62% | 0.063 | 0.034 | −0.015 | −0.147 | −0.347 | **0.814** | 0.311 | 0.371 | −0.514 | −0.231 |
| GD | | | | | | | | | | | |
| PC1 | 70.33% | **0.973** | **0.997** | **0.997** | **0.943** | **−0.824** | −0.315 | **0.935** | 0.468 | **0.828** | **−0.808** |
| PC2 | 29.67% | 0.231 | 0.074 | 0.083 | 0.334 | 0.567 | **0.949** | −0.355 | **0.884** | 0.561 | 0.59 |
| DD2 | | | | | | | | | | | |
| PC1 | 64.48% | 0.652 | 0.528 | 0.508 | **0.814** | **0.922** | 0.718 | **0.96** | **0.973** | **−0.847** | **0.985** |
| PC2 | 30.79% | 0.676 | **0.849** | **0.86** | 0.491 | −0.358 | −0.673 | −0.276 | −0.117 | 0.486 | −0.124 |
| FF | | | | | | | | | | | |
| PC1 | 65.00% | **0.956** | **0.93** | **0.951** | **0.927** | 0.154 | **0.786** | / | **0.913** | 0.003 | **0.914** |
| PC2 | 14.32% | −0.135 | −0.231 | −0.221 | 0.229 | **0.973** | −0.041 | / | −0.106 | −0.179 | 0.353 |
| PC3 | 11.40% | −0.142 | −0.02 | −0.086 | −0.036 | 0.156 | 0.176 | / | 0.102 | **0.965** | 0.012 |

Values in bold indicate factor loadings with |loading| > 0.7, representing the dominant variables contributing to each principal component.

### 3.2. Spatial Variation in $\delta^{18}O$

Figure 4 shows the variation in oxygen isotope ($\delta^{18}O$) in surface snow along five coastal transects of Antarctica, plotted versus distance from the coast. Because δD data are unavailable and δD and $\delta^{18}O$ exhibit consistent trends, δD is excluded from the analysis. Table 3 lists the minimum, mean, and maximum values of $\delta^{18}O$ for the five transects, together with the rates of change in $\delta^{18}O$ with increasing distance from the coast, altitude, and temperature. Surface snow $\delta^{18}O$ exhibits clear spatial differentiation with increasing distance from the coast. For all transects, $\delta^{18}O$ decreases with distance from the coast (Figure 4a–e). The ZL′ and VV transects on the northern flank of East Antarctica show a steep decline in $\delta^{18}O$, with rates ranging from −6.84 to −5.06‰/100 km (Table 3). For the ZL′ transect, $\delta^{18}O$ increases between the distance of 7.4 and 20.6 km from the coast (Figure 4a), indicating isotopic enrichment associated with strong uplift on the steep slope in that sector [34]. Beyond 20.6 km, $\delta^{18}O$ falls monotonically at a rate of −6.84‰/100 km. In contrast, the II transect in VL displays much gentler declines of −1.98‰/100 km, $R^2$ = 0.28. Lower explanatory power of models reveals the complexity of regional processes. The II and SS transects also differ markedly in amplitude, with $\delta^{18}O$ exhibiting abrupt fluctuations as distance from the coast increases (Figure 4c,d). Along the GD′ transect, $\delta^{18}O$ undergoes sharp oscillations within 50–150 km and then decreases steadily (Figure 4e), yielding an overall rate of −5.13‰/100 km with distance from the coast.

**Table 3.** Maximum, mean, and minimum values of $\delta^{18}O$, as well as the $\delta^{18}O$–distance gradient values.

| Transect | $\delta^{18}O$ (Minimum) | $\delta^{18}O$ (Mean) | $\delta^{18}O$ (Maximum) | $\delta^{18}O$–Distance (‰/100 km) | $\delta^{18}O$–Altitude (‰/100 m) | $\delta^{18}O$–Temperature (‰/°C) |
|---|---|---|---|---|---|---|
| ZL′ | −24.76 | −19.83 | −10.64 | −6.84 | −0.75 | 0.80 |
| VV | −40.25 | −32.32 | −19.03 | −5.06 | −0.97 | 0.89 |
| II | −44.29 | −41.09 | −36.42 | −1.98 | −0.49 | 0.96 |
| SS | −31.7 | −24.04 | −18.2 | −3.66 | −0.20 | 0.61 |
| GD′ | −36.47 | −27.26 | −18.57 | −5.13 | −0.53 | 1.14 |

The $\delta^{18}O$–altitude slope of surface snow across the five coastal transects exhibits marked vertical differentiation, ranging from −0.97 to −0.20‰/100 m (Table 3). The ZL′ and VV transects show the steepest gradients at −0.75‰/100 m and −0.97‰/100 m, respectively, indicating the strongest altitude dependence. The $\delta^{18}O$–altitude slopes of the II and GD′ transects are in the middle, being −0.49 and −0.53 respectively. In contrast, the gradients of the SS transect on the AP are much gentler at −0.20‰/100 m, $R^2$ = 0.19, indicating the weakest altitude dependence. These inter-transect slope differences point to marked regional variability in terms of the altitude effect on $\delta^{18}O$ along the Antarctic coast.

The slopes of the isotope–temperature relationship differ among the transects, ranging from 0.61 to 1.14 ‰/°C (Table 3). This range is generally consistent with the values (0.6–1.2‰/°C) reported in other studies conducted in Antarctica [17,42]. The ZL′ transect exhibits a $\delta^{18}O$–temperature slope of 0.80‰/°C, which is influenced by the steep topography that enhances local uplift and condensation processes, thereby increasing the sensitivity of $\delta^{18}O$ to temperature [43]. The $\delta^{18}O$–temperature slope for the VV transect is 0.89‰/°C, and the II transect shows a $\delta^{18}O$–temperature slope of 0.96‰/°C, while the GD′ transect has a slope of 1.14‰/°C (Table 3). The values exceed the spatial slope of 0.8‰/°C derived from the isotopic composition of Antarctic surface snow [17]. In contrast, the SS transect has a $\delta^{18}O$–temperature slope of 0.61‰/°C. The slopes of these five transects are consistent with the classical Dansgaard (2012) relation [42,44], indicating that $\delta^{18}O$ in these regions is controlled primarily by temperature.

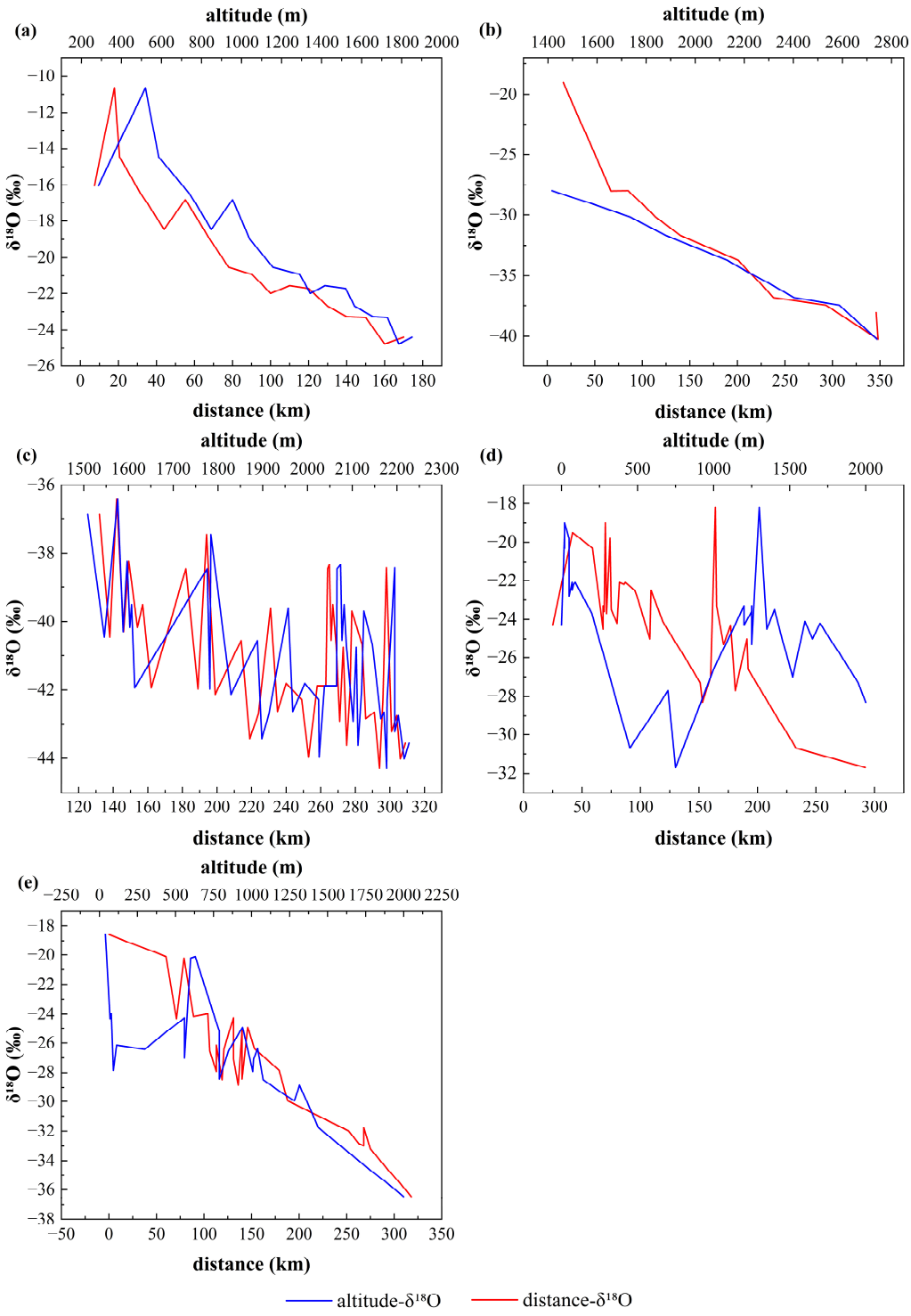


**Figure 4.** Variation in $\delta^{18}O$ with altitude and distance for each transect: (**a**) ZL′ transect, (**b**) VV transect, (**c**) II transect, (**d**) SS transect, (**e**) GD′ transect.

## 4. Discussion

### *4.1. Spatial Distribution and Source Analysis of Chemical Ions*

The spatial distributions of sea-salt ions ($Na^+$, $Cl^-$, $Mg^{2+}$, $K^+$) vary markedly, matching previous observations and reflecting the distance-dependent attenuation of marine aerosols (Figure 2). Sea-salt ion levels peak along the ZL transect on the East Antarctic coast and are lowest on the DD1 transect. In West Antarctica, the PV transect exhibits higher concentrations than the GD transect. A consistent feature is elevated sea-salt ion deposition

on steep cliffs, which likely results from local terrain effects on aerosol settling [45]. $Na^+$ is a typical sea-salt ion, and in these transects it conforms to the characteristic change in sea-salt ions, i.e., an exponential decrease with distance from the coast or with altitude. The EF values of $Cl^-$ and $Mg^{2+}$ are close to 1 for all transects, consistent with previous studies on the dominance of sea-salt aerosols in snow chemistry in coastal areas [35]. The special enrichment patterns of $K^+$ on the JJ, TT and FF transects might reflect selective fractionation during local terrigenous input or aerosol transport processes [46]. First, sea-salt fractionation during sea ice formation (particularly mirabilite precipitation at temperatures below −9 °C) can preferentially remove $Na^+$ and $SO_4^{2-}$, enriching residual sea-salt aerosols in $K^+$ and $Mg^{2+}$ relative to bulk seawater [22]. This process is active along Antarctic coasts during winter–spring and has been shown to elevate $K^+/Na^+$ ratios in aerosols and surface snow [35]. Second, terrestrial inputs from continental dust, possibly from Antarctic nunatak areas or long-range transport from southern South America, may contribute to $K^+$ enrichment at inland sites, where $K^+$ concentrations co-vary with crustal tracers such as Al [13]. These additional sources likely explain the transect-specific $K^+$ enrichment patterns observed in our study. The concentrations in East Antarctica are generally higher than those in West Antarctica, which is a pattern that correlates with regional differences in sea ice dynamics and marine aerosol transport [47]. Strong winds in East Antarctica likely enhance the long-range transport of sea-salt aerosols [48], whereas sea ice cover and local circulation patterns, such as the Amundsen Sea Low, appear to modulate sea-salt deposition in West Antarctica [16]. Markedly, sea-salt ions on the AP do not exhibit a clear gradient with altitude (Figure 2g), perhaps owing to complex topography and frequent resuspension of marine aerosols in that region.

The spatial distribution of non-sea-salt ions ($NO_3^-$, MSA, $SO_4^{2-}$, and $Ca^{2+}$) reflects contributions from distinct sources. $NO_3^-$ concentrations show no clear trend with distance from the coast or with altitude, supporting the stratospheric $NO_3^-$ hypothesis that purports that $NO_3^-$ distribution is not strongly controlled by either coastal proximity or altitude. MSA in the ZL transect of the East Antarctic (up to 146 ppb) is markedly higher than in West Antarctic sections (2–31 ppb on the GD transect), which departs from the West Antarctic biological dominance pattern reported by Masson-Delmotte et al. (2008) [17]. The high MSA concentrations observed along the ZL transect are consistent with enhanced biological productivity during the 2001/2002 austral summer. This period was characterized by anomalous atmospheric circulation that drove extensive sea ice melt and nutrient release, supporting large phytoplankton blooms [49]. Chlorophyll a concentrations in the Ross Sea during this season averaged 5.62–5.76 $\mu g L^{-1}$, with blooms peaking in December [50], conditions that are favorable for biogenic sulfur compound production and subsequent MSA deposition in coastal Antarctica. In the JJ transect, $nssSO_4^{2-}$ is enriched at high altitudes and attains higher concentrations than in other transects, consistent with the stratospheric sulfate input hypothesis of Wolff et al. (2006) [51]. This discrepancy might reflect intense summer algal blooms along the East Antarctic coast, whereas West Antarctic productivity is limited by sea ice cover [52]. Across the Antarctic coastal study area, $Ca^{2+}$ and $nssCa^{2+}$ concentrations remain low and stable, indicating input from long-range continental dust [34,53]. The enrichment of $Ca^{2+}$ and $SO_4^{2-}$ (EF > 1) reveals contributions of other important sources. Among them, $Ca^{2+}$ might originate mainly from mineral dust [35], while $SO_4^{2-}$ might be affected simultaneously by both marine biological emissions and long-range aerosol transport [40].

PCA further reveals the spatial differentiation of these source processes. PC1 accounts for the largest fraction of the variance (53–73.54%) in all transects, indicating that sea-salt aerosol deposition is a dominant process across the coastal region. PC2 explains the next largest share (14.4–31.1%), and its characteristic loadings include terrestrial indicators

($nssCa^{2+}$) and biogenic markers (MSA and $nssSO_4^{2-}$), reflecting spatial variability in non-sea-salt inputs. Differences in PCA patterns among transects—markedly the dominance of anomalous biogenic/terrestrial indicators in PC1 for the DD2 transect on the Antarctic Peninsula—might arise from the following factors: The exceptionally high $Ca^{2+}$ loading (0.985) is explained by the Peninsula's proximity to Patagonia, which has been identified as the primary dust source for this region: Pereira et al. (2004) showed that 95% of bulk-mode insoluble particulates deposited at King George Island originate from Chilean Patagonia, with cyclonic systems passing between southernmost South America and the Peninsula as the most probable transport mechanism [54]. The high MSA loading (0.96) reflects the biologically productive Weddell Sea, an important source of dimethyl sulphide; MSA concentrations in this sector are notably higher than elsewhere in Antarctica, with a mean molar MSA/$nssSO_4^{2-}$ ratio of 0.46 at Dolleman Island compared to 0.37–0.32 at other Peninsula sites [55]. The high $SO_4^{2-}$ loading (0.973) likely reflects a combination of marine biogenic emissions (via DMS oxidation) and additional sulfate from Patagonian dust [56]. The association of $SO_4^{2-}$ with both $Ca^{2+}$ and MSA in PC1 thus represents the convergence of two regionally enhanced source processes (continental dust transport and marine biogenic emissions) which are jointly stronger in the Peninsula sector than elsewhere along the Antarctic coast. The anomalous pattern observed on the DD2 transect warrants further investigation regarding how the region's unique geographic setting and local meteorological processes might influence aerosol deposition [57].

The factors regarding the differences in PCA patterns among transects can be summarized as follows: (1) variation in distance to biogenic hotspots (for example, the MSA signal of the ZL transect) [58]; (2) shifts in dust transport pathways, as seen in the terrestrial loading of the TT transect [59]; and (3) local microclimatic effects on aerosol chemical composition [37]. Although the PC3 contribution rate is relatively small and stable (11.4–13.6%), its association with atmospheric photochemical products ($NO_3^-$) indicates that chemical transformation processes are generally active on the Antarctic Peninsula [60]. These findings broadly support the classic model of Antarctic coastal aerosol chemistry while highlighting transect specificity driven by local environmental controls.

### *4.2. Spatial Variation in $\delta^{18}O$*

The characteristics of spatial variation in $\delta^{18}O$ of the surface snow at the five transects along the Antarctic coast reveal the complex interactions among water vapor transport, orographic uplift, and local climate processes. All transects show a trend of reduction in $\delta^{18}O$ with increasing distance from the coast, which is a pattern that closely matches published models of water vapor transport over the Antarctic ice sheet [61]. However, there are marked differences in the lapse rates ($-6.84$ to $-1.98$‰/100 km), reflecting the heterogeneity of water vapor source regions and precipitation processes in different areas [20]. The lapse rates in $\delta^{18}O$ of the ZL', VV and GD' transects on the coastland of Antarctica are the largest ($-6.84$ to $-5.06$‰/100 km), indicating that these areas are affected strongly by marine air masses and have marked isotope fractionation effects. In contrast, the changes in the II transect of VL are gentle ($-1.98$‰/100 km), which might be related to its relatively stable local circulation [62]. Markedly, there is enrichment of $^{18}O$ on the ZL' transect within the range of 0–20.6 km (Figure 4a), and this anomaly likely arises from the preferential loss of lighter isotopes through raindrop evaporation and snow sublimation during intense orographic precipitation, leaving the residual snow enriched in heavy isotopes. It should be noted, however, that no concurrent temperature or humidity measurements are available to verify the occurrence of raindrop evaporation. Additionally, the high local accumulation rate suggests that the surface snow samples may have captured an extreme precipitation event with anomalously elevated $\delta^{18}O$ values [8].

Furthermore, the abrupt topography may have induced a shift in the moisture source within precipitating clouds, from lower-level, near-source air masses to upper-level advected vapor with inherently higher $\delta^{18}O$ baselines. These combined effects underscore the strong modulation of isotopic fractionation by orographic forcing and local vapor exchange in steep coastal zones [61].

The spatial variability of the $\delta^{18}O$–altitude slope (−0.97 to −0.20‰/100 m) underscores regional differences in the altitude effect across Antarctic coastal areas [63]. The steepest slopes on the ZL′ and VV transects align with enhanced condensation efficiency driven by strong orographic uplift. In contrast, the gentler slopes on the SS transect of the AP likely reflect inhibition of air mass transport by subdued terrain.

The relationship between $\delta^{18}O$ and temperature (0.61–1.14‰/°C) generally falls within the classic Antarctic spatial slope range (0.6–1.20‰/°C) [42,43], but differences among transects highlight the influence of local processes. The high slopes (0.89–1.14‰/°C) observed for the VV, II and GD′ transects exceed the reported spatial slope for Antarctic surface snow (0.8‰/°C) [17], implying that $\delta^{18}O$ in these regions is unusually sensitive to temperature changes, possibly because stable precipitation under a strong maritime climate preserves the primary temperature signal. In contrast, the low slopes (0.61‰/°C) on the SS transect likely reflect local secondary evaporation or the mixing of different air masses, which attenuates the original isotope–temperature relationship. The intermediate slope (0.80‰/°C) of the ZL′ transect suggests that steep terrain partially counteracts temperature-driven isotope fractionation by enhancing orographic uplift and condensation [43].

The distribution of $\delta^{18}O$ along the Antarctic coast is governed by three main factors: (1) moisture source regions and transport pathways, which impose a broad "distance-from-coast" constraint on $\delta^{18}O$; (2) orographic uplift, which modifies the altitude-dependence by changing air mass condensation efficiency; and (3) the local temperature field, whose influence on $\delta^{18}O$ is mediated by the topography and microclimate [38].

## 5. Conclusions

This study analyzed the similarities and differences in chemical ion variation across eight Antarctic coastal surface snow transects, focusing on spatial distribution and source attribution. Furthermore, the spatial distribution characteristics of $\delta^{18}O$ across five transects were investigated, focusing on the influences of distance, altitude, and temperature. The main conclusions derived are as follows.

1. Concentrations of sea-salt ions ($Na^+$, $Cl^-$, $Mg^{2+}$, and $K^+$) in East Antarctica are generally higher than in West Antarctica, and this pattern correlates with regional differences in sea ice dynamics and marine aerosol transport. The non-sea-salt ions ($NO_3^-$, MSA, $SO_4^{2-}$, and $Ca^{2+}$) exhibit distinct source signatures.
2. The EF values indicate that $Cl^-$ and $Mg^{2+}$ are derived mainly from marine aerosols, while $nssSO_4^{2-}$ and $nssCa^{2+}$ have opposite sources, and $K^+$ has both sea-salt and non-sea-salt sources. PCA further indicates that in the coastal areas of Antarctica, the ranking of ion sources is as follows: sea-salt aerosol transport, followed by marine biological activities and long-distance transported mineral dust and then atmospheric chemical reactions.
3. All transects share the general pattern of decreasing $\delta^{18}O$ with increasing distance from the coast, but the rate of change varies markedly (−6.84 to −1.98‰/100 km). Moreover, the isotopic variation trends of the II, SS and GD′ transects fluctuate sharply with the increase in distance from the sea, indicating the strong influence of the local microclimate and topography on stable isotope distributions. Transects on the coastal areas of Antarctica (ZL′, VV, GD′) display the strongest isotopic altitude effect, whereas the SS transect on the AP shows weaker responses.

4. The high $\delta^{18}O$–temperature slopes (0.96 to 1.14‰/°C) observed for the II and GD′ transects suggest that $\delta^{18}O$ in these regions is unusually sensitive to temperature changes, possibly because stable precipitation under a strong maritime climate preserves the primary temperature signal. The SS transect shows lower temperature sensitivity (0.61‰/°C), suggesting locally enhanced air mass mixing or evaporation effects.

This study had primary limitations. First, the surface snow dataset spans a long period, which makes it difficult to eliminate the effects of short-term meteorological events (e.g., blizzards) and might introduce interannual climate variability (e.g., ENSO). Second, the sampling dates for some transects (e.g., DD1 and FF) are unclear, which might produce seasonal bias. Third, the attribution of $\delta^{18}O$ variability to local processes is qualitative, as no trajectory or modeling analyses were performed.

This study characterized the spatial differentiation patterns of substances in the Antarctic coastal environment and determined how they are derived, and its findings provide new data and a theoretical framework for studying polar biogeochemical cycles. The presented paradigm, i.e., that local processes dominate regional differences, could be utilized to predict polar amplification under the effects of global climate change.

**Author Contributions:** Conceptualization, Y.D. and M.Y.; methodology, M.Y., Y.D. and W.H.; software, M.Y., R.M., C.A., L.L., Y.D. and W.H.; validation, M.Y., Z.C., Y.D. and W.H.; investigation, M.Y., Z.C., C.A. and L.L.; resources, M.Y.; data curation, M.Y., R.M. and Y.D.; writing—original draft preparation, Y.D.; writing—review and editing, M.Y., Z.C., Y.D. and W.H.; supervision, M.Y. and Z.C.; project administration, M.Y.; funding acquisition, M.Y. All authors have read and agreed to the published version of the manuscript.

**Funding:** This research was supported by the National Natural Science Foundation of China (41676192; 42376242).

**Data Availability Statement:** The original contributions presented in this study are included in the article. Further inquiries can be directed to the corresponding authors. The data used in this study were compiled from three sources: (1) the ITASE surface snow chemistry database (http://www2.umaine.edu/itase/content/syngroups/snowchem.html (accessed on 23 March 2026)), which provided ion concentration data for the eight chemical transects (JJ, TT, DD1, PV, GD, DD2, FF); (2) the Antarctic surface snow isotope composition database (https://doi.pangaea.de/10.1594/PANGAEA.681697, (accessed on 23 March 2026)), which provided $\delta^{18}O$ data for four of the five isotope transects (VV, II, SS, GD′); and (3) our own field measurements from the 18th CHINARE (Chinese Antarctic Research Expedition, 2001–2002) along the Zhongshan–LGB69 transect, which provided both chemical and isotope data for the ZL/ZL′ transect.

**Conflicts of Interest:** The authors declare no conflicts of interest.

## Abbreviations

The following abbreviations are used in this manuscript:

| | |
|---|---|
| DML | Dronning Maud Land |
| EL | Enderby Land |
| PEL | Princess Elizabeth Land |
| KWL | Kaiser Wilhelm II Land |
| MBL | Marie Byrd Land |
| AL | Adélie Land |
| VL | Victoria Land |
| AP | Antarctic Peninsula |
| JJ | Japan96-Japan114 |
| ZL | Zhongshan–LGB69 |

| | |
|---|---|
| TT | T.-Talos_Dome |
| DD1 | D42-D80 |
| PV | pp-VLG1 |
| GD | Gl-CWA_D |
| DD2 | Dolleman Is.-DML |
| FF | Finland1-Findland17 |
| GD′ | GvN 2 km Süd-DML75 |
| ZL′ | Zhongshan–LGB69 |
| VV | Vostok1385-Vostok1033 |
| II | ITS7-ITS63 |
| SS | site1-site31 |

## References


1. Espinosa, Z.I.; Blanchard-Wrigglesworth, E.; Bitz, C.M. Understanding the Drivers and Predictability of Record Low Antarctic Sea Ice in Austral Winter 2023. *Commun. Earth Environ.* **2024**, *5*, 723. [CrossRef]
2. Legrand, M.; Mayewski, P. Glaciochemistry of Polar Ice Cores: A Review. *Rev. Geophys.* **1997**, *35*, 219–243. [CrossRef]
3. Domine, F.; Sparapani, R.; Ianniello, A.; Beine, H.J. The Origin of Sea Salt in Snow on Arctic Sea Ice and in Coastal Regions. *Atmos. Chem. Phys.* **2004**, *4*, 2259–2271. [CrossRef]
4. Wolff, E.W.; Rankin, A.M.; Röthlisberger, R. An Ice Core Indicator of Antarctic Sea Ice Production? *Geophys. Res. Lett.* **2003**, *30*, 2003GL018454. [CrossRef]
5. Arimoto, R.; Nottingham, A.S.; Webb, J.; Schloesslin, C.A.; Davis, D.D. Non-Sea Salt Sulfate and Other Aerosol Constituents at the South Pole During ISCAT. *Geophys. Res. Lett.* **2001**, *28*, 3645–3648. [CrossRef]
6. Legrand, M.R.; Kirchner, S. Origins and Variations of Nitrate in South Polar Precipitation. *J. Geophys. Res.* **1990**, *95*, 3493–3507. [CrossRef]
7. Shi, G.; Hastings, M.G.; Yu, J.; Ma, T.; Hu, Z.; An, C.; Li, C.; Ma, H.; Jiang, S.; Li, Y. Nitrate Deposition and Preservation in the Snowpack Along a Traverse from Coast to the Ice Sheet Summit (Dome A) in East Antarctica. *Cryosphere* **2018**, *12*, 1177–1194. [CrossRef]
8. Jackson, S.L.; Vance, T.R.; Crockart, C.; Moy, A.; Plummer, C.; Abram, N.J. Climatology of the Mount Brown South Ice Core Site in East Antarctica: Implications for the Interpretation of a Water Isotope Record. *Clim. Past.* **2023**, *19*, 1653–1675. [CrossRef]
9. Gao, Q.; Sime, L.C.; McLaren, A.J.; Werner, M. Moisture Source Controls on Water Isotopes in Antarctic Precipitation—Insights From Water Tracers in ECHAM6-Wiso. *J. Geophys. Res. Atmos.* **2025**, *130*, e2024JD043047. [CrossRef]
10. Bertler, N.; Mayewski, P.A.; Aristarain, A.; Barrett, P.; Becagli, S.; Bernardo, R.; Bo, S.; Xiao, C.; Curran, M.; Qin, D.; et al. Snow Chemistry Across Antarctica. *Ann. Glaciol.* **2005**, *41*, 167–179. [CrossRef]
11. Shi, G.; Ma, H.; Hu, Z.; Chen, Z.; An, C.; Jiang, S.; Li, Y.; Ma, T.; Yu, J.; Wang, D.; et al. Brief Communication: Spatial and Temporal Variations in Surface Snow Chemistry Along a Traverse from Coastal East Antarctica to the Ice Sheet Summit (Dome A). *Cryosphere* **2021**, *15*, 1087–1095. [CrossRef]
12. Proposito, M.; Becagli, S.; Castellano, E.; Flora, O.; Genoni, L.; Gragnani, R.; Stenni, B.; Traversi, R.; Udisti, R.; Frezzotti, M. Chemical and Isotopic Snow Variability Along the 1998 ITASE Traverse from Terra Nova Bay to Dome C, East Antarctica. *Ann. Glaciol.* **2002**, *35*, 187–194. [CrossRef]
13. Khodzher, T.V.; Golobokova, L.P.; Osipov, E.Y.; Shibaev, Y.A.; Lipenkov, V.Y.; Osipova, O.P.; Petit, J.R. Spatial–Temporal Dynamics of Chemical Composition of Surface Snow in East Antarctica Along the Progress Station–Vostok Station Transect. *Cryosphere* **2014**, *8*, 931–939. [CrossRef]
14. Iizuka, Y.; Ohno, H.; Uemura, R.; Suzuki, T.; Oyabu, I.; Hoshina, Y.; Fukui, K.; Hirabayashi, M.; Motoyama, H. Spatial Distributions of Soluble Salts in Surface Snow of East Antarctica. *Tellus B Chem. Phys. Meteorol.* **2016**, *68*, 29285. [CrossRef]
15. Kreutz, K.J.; Mayewski, P.A. Spatial Variability of Antarctic Surface Snow Glaciochemistry: Implications for Palaeoatmospheric Circulation Reconstructions. *Antart. Sci.* **1999**, *11*, 105–118. [CrossRef]
16. Kreutz, K.J.; Mayewski, P.A.; Pittalwala, I.I.; Meeker, L.D.; Twickler, M.S.; Whitlow, S.I. Sea Level Pressure Variability in the Amundsen Sea Region Inferred from a West Antarctic Glaciochemical Record. *J. Geophys. Res.* **2000**, *105*, 4047–4059. [CrossRef]
17. Masson-Delmotte, V.; Hou, S.; Ekaykin, A.; Jouzel, J.; Aristarain, A.; Bernardo, R.T.; Bromwich, D.; Cattani, O.; Delmotte, M.; Falourd, S.; et al. A Review of Antarctic Surface Snow Isotopic Composition: Observations, Atmospheric Circulation, and Isotopic Modeling. *J. Clim.* **2008**, *21*, 3359–3387. [CrossRef]
18. Heil, P.; Stevens, C.; Lee, W.S.; Eayrs, C.; Shin, H.C.; Alexander, S.P.; Rack, W. Bridging the Gap for Ice–Ocean–Ecosystem Processes: Integrated Observing System for the Ross Sea-Far East Antarctic Region. *Front. Mar. Sci.* **2023**, *10*, 1206119. [CrossRef]

19. Mulvaney, R.; Wolff, E.W. Spatial Variability of the Major Chemistry of the Antarctic Ice Sheet. *Ann. Glaciol.* **1994**, *20*, 440–447. [CrossRef]
20. Ding, M.; Xiao, C.; Jin, B.; Ren, J.; Qin, D.; Sun, W. Distribution of $\delta^{18}O$ in Surface Snow Along a Transect from Zhongshan Station to Dome A, East Antarctica. *Chin. Sci. Bull.* **2010**, *55*, 2709–2714. [CrossRef]
21. Giordano, M.R.; Kalnajs, L.E.; Goetz, J.D.; Avery, A.M.; Katz, E.; May, N.W.; Leemon, A.; Mattson, C.; Pratt, K.A.; DeCarlo, P.F. The Importance of Blowing Snow to Halogen-Containing Aerosol in Coastal Antarctica: Influence of Source Region Versus Wind Speed. *Atmos. Chem. Phys.* **2018**, *18*, 16689–16711. [CrossRef]
22. Hara, K.; Osada, K.; Yabuki, M.; Matoba, S.; Hirabayashi, M.; Fujita, S.; Nakazawa, F.; Yamanouchi, T. Atmospheric Sea-Salt and Halogen Cycles in the Antarctic. *Environ. Sci. Process. Impacts* **2020**, *22*, 2003–2022. [CrossRef] [PubMed]
23. Williamson, B.R.; Kreutz, K.J.; Mayewski, P.A.; Bertler, N.A.N.; Sneed, S.; Handley, M.; Introne, D. A Coastal Transect of McMurdo Dry Valleys (Antarctica) Snow and Firn: Marine and Terrestrial Influences on Glaciochemistry. *J. Glaciol.* **2007**, *53*, 681–693. [CrossRef]
24. Frey, M.M.; Norris, S.J.; Brooks, I.M.; Anderson, P.S.; Nishimura, K.; Yang, X.; Jones, A.E.; Mastromonaco, M.G.N.; Jones, D.H.; Wolff, E.W. First Direct Observation of Sea Salt Aerosol Production from Blowing Snow Above Sea Ice. *Atmos. Chem. Phys.* **2020**, *20*, 2549–2578. [CrossRef]
25. Kim, S.; Han, Y.; Chung, J.; Ro, S.; Moon, J.; Hur, S.D.; Lee, J. Imprints of Sea Ice, Wind Patterns, and Atmospheric Systems on Summer Water Isotope Signatures at Hercules Névé, East Antarctica. *Cryosphere* **2025**, *19*, 5655–5670. [CrossRef]
26. Boutron, C.; Lorius, C. Trace Element Content in East Antarctica Snow Samples. In *Isotopes and Impurities in Snow and Ice*; IAHS Publication 118; International Association of Hydrological Sciences: Wallingford, UK, 1977; pp. 164–171.
27. Ekaykin, A.A.; Lipenkov, V.Y.; Barkov, N.I.; Petit, J.R.; Masson-Delmotte, V. Spatial and Temporal Variability in Isotope Composition of Recent Snow in the Vicinity of Vostok Station, Antarctica: Implications for Ice-Core Record Interpretation. *Ann. Glaciol.* **2002**, *35*, 181–186. [CrossRef]
28. Lipenkov, V.; Ekaykin, A.A.; Barkov, N.I.; Pourchet, M. On the Relation between Surface Snow Density in Antarctica and Wind Speed. *Data Glaciol. Stud.* **1998**, *85*, 148–158.
29. Frezzotti, M.; Pourchet, M.; Flora, O.; Gandolfi, S.; Gay, M.; Urbini, S.; Vincent, C.; Becagli, S.; Gragnani, R.; Proposito, M.; et al. Spatial and Temporal Variability of Snow Accumulation in East Antarctica from Traverse Data. *J. Glaciol.* **2005**, *51*, 113–124. [CrossRef]
30. Dahe, Q.; Petit, J.R.; Jouzel, J.; Stievenard, M. Distribution of Stable Isotopes in Surface Snow along the Route of the 1990 International Trans-Antarctica Expedition. *J. Glaciol.* **1994**, *40*, 107–118. [CrossRef]
31. Graf, W.; Moser, H.; Reinwarth, O.; Kipfstuhl, J.; Oerter, H.; Minikin, A.; Wagenbach, D. Snow-Accumulation Rates and Isotopic Content (2 H,3 H) of near-Surface Firn from the Filchner-Ronne Ice Shelf, Antarctica. *Ann. Glaciol.* **1994**, *20*, 121–128. [CrossRef]
32. Oerter, H.; Graf, W.; Wilhelms, F.; Minikin, A.; Miller, H. Accumulation Studies on Amundsenisen, Dronning Maud Land, Antarctica, by Means of Tritium, Dielectric Profiling and Stable-Isotope Measurements: First Results from the 1995–1996 and 1996–97 Field Seasons. *Ann. Glaciol.* **1999**, *29*, 1–9. [CrossRef]
33. Graf, W.; Moser, H.; Oerter, H.; Reinwarth, O.; Stichler, W. Accumulation and Ice-Core Studies on Filchner-Ronne Ice Shelf, Antarctica. *Ann. Glaciol.* **1988**, *11*, 23–31. [CrossRef]
34. Huang, W.; Yan, M.; Mulvaney, R.; Qian, Z.; Liu, L.; An, C.; Xiao, C.; Zhang, Y. Spatial Variability of Glaciochemistry Along a Transect from Zhongshan Station to LGB69, Antarctica. *Atmosphere* **2021**, *12*, 393. [CrossRef]
35. Thamban, M.; Laluraj, C.M.; Mahalinganathan, K.; Redkar, B.L.; Naik, S.S.; Shrivastava, P.K. Glaciochemistry of Surface Snow from the Ingrid Christensen Coast, East Antarctica, and Its Environmental Implications. *Antarct. Sci.* **2010**, *22*, 435–441. [CrossRef]
36. Lawson, D.R.; Winchester, J.W. A Standard Crustal Aerosol as a Reference for Elemental Enrichment Factors. *Atmos. Environ. (1967)* **1979**, *13*, 925–930. [CrossRef]
37. Osipov, E.Y.; Osipova, O.P.; Khodzher, T.V. Recent Variability of Atmospheric Circulation Patterns Inferred from East Antarctica Glaciochemical Records. *Geochemistry* **2020**, *80*, 125554. [CrossRef]
38. Hou, S.; Wang, Y.; Pang, H. Climatology of Stable Isotopes in Antarctic Snow and Ice: Current Status and Prospects. *Chin. Sci. Bull.* **2013**, *58*, 1095–1106. [CrossRef]
39. Göktas, F.; Fischer, H.; Oerter, H.; Weller, R.; Sommer, S.; Miller, H. A Glacio-Chemical Characterization of the New EPICA Deep-Drilling Site on Amundsenisen, Dronning Maud Land, Antarctica. *Ann. Glaciol.* **2002**, *35*, 347–354. [CrossRef]
40. Becagli, S.; Proposito, M.; Benassai, S.; Gragnani, R.; Magand, O.; Traversi, R.; Udisti, R. Spatial Distribution of Biogenic Sulphur Compounds (MSA, $nssSO_4^{2-}$) in the Northern Victoria Land–Dome C–Wilkes Land Area, East Antarctica. *Ann. Glaciol.* **2005**, *41*, 23–31. [CrossRef]
41. Becagli, S.; Barbaro, E.; Bonamano, S.; Caiazzo, L.; Di Sarra, A.; Feltracco, M.; Grigioni, P.; Heintzenberg, J.; Lazzara, L.; Legrand, M.; et al. Factors Controlling Atmospheric DMS and Its Oxidation Products (MSA and $nssSO_4^{2-}$) in the Aerosol at Terra Nova Bay, Antarctica. *Atmos. Chem. Phys.* **2022**, *22*, 9245–9263. [CrossRef]

42. Casado, M.; Bailey, A.; Leroy-Dos Santos, C.; Fourré, E.; Favier, V.; Agosta, C.; Dutrievoz, N.; Kittel, C.; Arnaud, L.; Prié, F.; et al. Water Isotope–Temperature Relationship Variability Across Antarctica Set by Atmospheric Circulation. *Nat. Geosci.* **2026**, *19*, 581–588. [CrossRef] [PubMed]
43. Yan, M.; Li, Y.; Hammer, C.U.; Gundestrup, N.S.; Tan, D.; Wen, J.; Wang, D.; Sun, B.; Kang, J.; Liu, L. Oxygen Isotope Composition of Surface Snow Collected Along the Traverse Route from Zhongshan Station Toward Dome A, Antarctica. *Polar Meteorol. Glaciol.* **2002**, *16*, 133–139.
44. Dansgaard, W. Stable Isotopes in Precipitation. *Tellus A Dyn. Meteorol. Oceanogr.* **2012**, *16*, 436–438.
45. Mahalinganathan, K.; Thamban, M.; Laluraj, C.M.; Redkar, B.L. Relation Between Surface Topography and Sea-Salt Snow Chemistry from Princess Elizabeth Land, East Antarctica. *Cryosphere* **2012**, *6*, 505–515. [CrossRef]
46. Cini, R.; Udisti, R.; Piccardi, G.; Loglio, G.; Innocenti, N.D.; Stortini, A.M.; Pampaloni, B.; Tesei, U. A Simple Model for K and Ca Enrichment Interpretation in Antarctic Snow. *Int. J. Environ. Anal. Chem.* **1998**, *71*, 265–287. [CrossRef]
47. Qin, D.; Mayewski, P.A.; Ren, J.; Xiao, C.; Sun, J. The Weddell Sea Region: An Important Precipitation Channel to the Interior of the Antarctic Ice Sheet as Revealed by Glaciochemical Investigation of Surface Snow Along the Longest Trans-Antarctic Route. *Ann. Glaciol.* **1999**, *29*, 55–60. [CrossRef]
48. Hara, K.; Nakazawa, F.; Fujita, S.; Fukui, K.; Enomoto, H.; Sugiyama, S. Horizontal Distributions of Aerosol Constituents and Their Mixing States in Antarctica during the JASE Traverse. *Atmos. Chem. Phys.* **2014**, *14*, 10211–10230. [CrossRef]
49. Massom, R.A.; Stammerjohn, S.E.; Smith, R.C.; Pook, M.J.; Iannuzzi, R.A.; Adams, N.; Martinson, D.G.; Vernet, M.; Fraser, W.R.; Quetin, L.B.; et al. Extreme Anomalous Atmospheric Circulation in the West Antarctic Peninsula Region in Austral Spring and Summer 2001/02, and Its Profound Impact on Sea Ice and Biota*. *J. Clim.* **2006**, *19*, 3544–3571. [CrossRef]
50. Peloquin, J.A.; Smith, W.O. Phytoplankton Blooms in the Ross Sea, Antarctica: Interannual Variability in Magnitude, Temporal Patterns, and Composition. *J. Geophys. Res.* **2007**, *112*, 2006JC003816. [CrossRef]
51. Wolff, E.W.; Fischer, H.; Fundel, F.; Ruth, U.; Twarloh, B.; Littot, G.C.; Mulvaney, R.; Röthlisberger, R.; De Angelis, M.; Boutron, C.F.; et al. Southern Ocean Sea-Ice Extent, Productivity and Iron Flux over the Past Eight Glacial Cycles. *Nature* **2006**, *440*, 491–496. [CrossRef] [PubMed]
52. Ducklow, H.; Fraser, W.; Meredith, M.; Stammerjohn, S.; Doney, S.; Martinson, D.; Sailley, S.; Schofield, O.; Steinberg, D.; Venables, H.; et al. West Antarctic Peninsula: An Ice-Dependent Coastal Marine Ecosystem in Transition. *Oceanography* **2013**, *26*, 190–203. [CrossRef]
53. Mahalinganathan, K.; Thamban, M. Potential Genesis and Implications of Calcium Nitrate in Antarctic Snow. *Cryosphere* **2016**, *10*, 825–836. [CrossRef]
54. Pereira, K.C.D.; Evangelista, H.; Pereira, E.B.; Simoes, J.C.; Johnson, E.; Melo, L.R. Transport of Crustal Microparticles from Chilean Patagonia to the Antarctic Peninsula by SEM-EDS Analysis. *Tellus B* **2004**, *56*, 262–275. [CrossRef]
55. Mulvaney, R.; Pasteur, E.C.; Peel, D.A.; Saltzman, E.S.; Whung, P.-Y. The Ratio of MSA to Non-Sea-Salt Sulphate in Antarctic Peninsula Ice Cores. *Tellus B* **1992**, *44*, 295–303. [CrossRef]
56. Artaxo, P.; Rabello, M.L.C.; Maenhaut, W.; Grieken, R.V. Trace Elements and Individual Particle Analysis of Atmospheric Aerosols from the Antarctic Peninsula. *Tellus B* **1992**, *44*, 318–334. [CrossRef]
57. Xie, Z.; Sun, L.; Wang, J.; Liu, B. A Potential Source of Atmospheric Sulfur from Penguin Colony Emissions. *J. Geophys. Res. Atmos.* **2002**, *107*, ACH 5-1–ACH 5-10. [CrossRef]
58. Yu, J.; Li, Y.; Ma, H.; Shi, G.; Ma, T.; An, C.; Jiang, S. Spatial Distribution Characteristics of $SO_4^{2-}$ and MSA in Surface Snow Along the Traverse Route from Zhongshan Station to Dome A, East Antarctica. *Chin. J. Polar Res.* **2017**, *29*, 45–55.
59. Du, Z.; Xiao, C.; Ding, M.; Li, C. Identification of Multiple Natural and Anthropogenic Sources of Dust in Snow from Zhongshan Station to Dome A, East Antarctica. *J. Glaciol.* **2018**, *64*, 855–865. [CrossRef]
60. Shi, G.; Buffen, A.M.; Ma, H.; Hu, Z.; Sun, B.; Li, C.; Yu, J.; Ma, T.; An, C.; Jiang, S.; et al. Distinguishing Summertime Atmospheric Production of Nitrate Across the East Antarctic Ice Sheet. *Geochim. Cosmochim. Acta* **2018**, *231*, 1–14. [CrossRef]
61. Liu, J.; Du, Z.; Zhang, D.; Wang, S. Diagnoses of Antarctic Inland Water Cycle Regime: Perspectives from Atmospheric Water Vapor Isotope Observations Along the Transect From Zhongshan Station to Dome A. *Front. Earth Sci.* **2022**, *10*, 823515. [CrossRef]
62. Arnold, M. Surface Mass Balance of the Ross Ice Shelf from Stable Water Isotopes, Ground Penetrating Radar, and Back Trajectory Analyses. Master's Thesis, University of Canterbury, Christchurch, New Zealand, 2016.
63. Smith, B.T.; Van Ommen, T.D.; Morgan, V.I. Distribution of Oxygen Isotope Ratios and Snow Accumulation Rates in Wilhelm II Land, East Antarctica. *Ann. Glaciol.* **2002**, *35*, 107–110. [CrossRef]